Fiber density of electrospun gelatin scaffolds regulates morphogenesis of dermal–epidermal skin substitutes

H. M. Powell,[1] S. T. Boyce[1,2]
[1]*Research Department, Shriners Burns Hospital, 3229 Burnet Ave., Cincinnati, Ohio 45229*
[2]*Department of Surgery, College of Medicine, University of Cincinnati, 2314 Albert Sabin Way, Cincinnati, Ohio 45249*

Received 26 September 2006; revised 9 March 2007; accepted 4 May 2007
Published online 8 August 2007 in Wiley InterScience (www.interscience.wiley.com). DOI: 10.1002/jbm.a.31498

Abstract: Porous, nowoven fibrous gelatin scaffolds were prepared using electrospinning. Electrospun scaffolds with varying fiber diameter, interfiber distance, and porosity were fabricated by altering the concentration of the electrospinning solution. Solution concentration was a significant predictor of fiber diameter, interfiber distance, and porosity with higher solution concentration correlated with larger fiber diameters and interfiber distances. The potential of electrospun gelatin as a scaffolding material for dermal and epidermal tissue regeneration was also evaluated. Interfiber distances >5.5 μm allowed deeper penetration of human dermal fibroblasts into the scaffold, whereas cells in scaffolds with more densely packed fibers were able to infiltrate only into the upper regions. Scaffolds with interfiber distances $\leq$10 μm exhibited well-stratified dermal and epidermal layers including a continuous basal keratinocyte layer. These scaffolds were shown to form a keratinized layer like in normal skin, which acts as a barrier to infection and fluid loss. Interfiber distances between 5 and 10 μm appear to yield the most favorable skin substitute *in vitro*, demonstrating high cell viability, optimal cell organization, and excellent barrier formation. These results demonstrate the feasibility of electrospun gelatin as a scaffold for dermal–epidermal composite skin substitutes. © 2007 Wiley Periodicals, Inc. J Biomed Mater Res 84A: 1078–1086, 2008

Key words: tissue engineering; skin; electrospinning; gelatin; scaffold; wound healing

INTRODUCTION

Scaffolds for tissue engineering play a critical role in regenerating functional tissues and organs. Ideally, a scaffold will provide a substitute extracellular matrix (ECM) upon which cells can attach, proliferate, and organize as in natural tissue. It is generally recognized that both biochemical composition and microstructure of the scaffold affect cellular activity and organization.[1]

As the native ECM is comprised largely of proteins from the collagen family, emphasis has been placed on fabricating scaffolds from collagen and collagen-based composites.[2–4] Gelatin, a biopolymer derived from native collagens, is potentially useful as a scaffolding material due to its low immunogenicity, biodegradability, biocompatibility, and low cost. Gelatin is widely used as a dressing for wound healing[5–9] and as a scaffold for dermal tissue engineering.[10–12] Gelatin can be formed via electrospinning into fibrous scaffolds at a scale similar to native ECM, which makes these scaffolds conducive for tissue engineering.[5,13,14] Electrospun gelatin and gelatin blends have been previously shown to support the growth of human embryonic palatal mesenchymal cells[15] and rat cardiac myoblasts.[16] Acellular electrospun gelatin tubes have also been implanted into the belly of the vastus lateralis of rats[17] and were associated with a large inflammatory response. Acellular gelatin sponges used as wound dressings have also been associated with acute inflammatory responses in a wound healing model.[9] However, if these sponges were populated with fibroblasts no significant negative immune response was detected and the wounds were re-epithelialized within 2 weeks.[9] Thus, the use of electrospun gelatin scaffolds for a skin substitute model containing high densities of both fibroblasts and keratinocytes is not expected to elicit an acute inflammatory response if used *in vivo*.

In addition to material composition, pore size, pore orientation, fiber structure and fiber diameter of scaffolds affect proliferation, cellular organization, and subsequent tissue morphogenesis.[18–21] Scaffold pore

Correspondence to: H. M. Powell; e-mail: hpowell@shrinenet.org
Contract grant sponsor: Shriners Hospitals for Children; contract grant numbers: 8450 and 9507

size influences cell morphology and phenotypic expression,[22–24] the extent of cell migration,[25] DNA synthesis,[23] and tissue ingrowth.[26] Proper regulation of scaffold pore size has been reported to control wound contraction in full-thickness dermal defects.[27] Scaffold fiber diameter has also been shown to affect cellular behavior. For example, nanofibrous chitin scaffolds exhibited an increase in fibroblast and keratinocyte attachment and spreading compared with a commercially available microfibrous chitin scaffold.[28] The preferred scaffold morphology is dependent on cell type and target tissue to be repaired.[25,29–32]

The lack of sufficient donor sites for the harvesting of split-thickness autografts to treat extensive burn injuries is a major impetus for designing bioengineered skin. Tissue engineering has been utilized to generate bioengineered skin replacements which generate greater surface area expansion from donor skin than conventional methods.[33] The majority of bioengineered skin substitutes are comprised of freeze-dried biopolymer sponges populated with dermal fibroblasts alone[34,35] or in conjunction with keratinocytes.[36–38] However, freeze-drying is a labor intensive, costly process that can produce sponges with significant structural heterogeneity.[1,39] To overcome these difficulties, electrospinning has been used to generate nonwoven, homogeneous fibrous scaffolds from a wide variety of synthetic and natural polymers.

The purpose of this study is to determine an optimal morphology for an electrospun scaffold for skin repair. Electrospun gelatin scaffolds were fabricated with varying degrees of porosity, fiber diameter, and interfiber distance. The physical properties of the scaffolds were evaluated prior to cell inoculation and the ability of the scaffold to support cell proliferation, organization, and maturation was evaluated.

MATERIALS AND METHODS

Gelatin scaffolds

Nonwoven, fibrous gelatin scaffolds were prepared by electrospinning a solution of gelatin type B (Sigma, St. Louis, MO) and 2,2,2-trifluoroethanol (TFE; Sigma) at 10, 12, 14, or 16 wt/vol %. Solutions were electrospun onto a 9×9 cm^2 grounding plate covered with aluminum foil at a feed velocity and electrical potential of 8 mL/h and 28 kV for the 10% solution and 12 mL/h and 26 kV for 12–16% solutions. Scaffolds were fabricated at an average thickness of 200 μm by controlling the volume of solution spun onto the grounding plate. Gelatin scaffolds were physically crosslinked by vacuum dehydration[40] at 140°C and −100 kPa for 24 h then chemically cross-linked for 24 h at room temperature in 7 m*M* 1-ethyl-3-3-dimethylaminopropylcarbodiimide hydrochloride (EDC) in pure ethanol. Scaffolds were disinfected in 70% ethanol for 24 h, rinsed twice for 24 h with phosphate buffer solution (PBS; Sigma), four times for 15–20 min with Hepes-buffered saline (HBS) solution, and twice for 15–20 min with cell culture medium (UCMC 160)[41] prior to cell inoculation.

Scanning electron microscopy

The morphology of each group of gelatin scaffolds was examined via scanning electron microscopy (Hitachi S-3000). Dry, as-spun gelatin scaffolds were mounted onto aluminum stubs, sputter coated with gold–palladium, and imaged in secondary electron mode with a 5 kV accelerating voltage. Fiber diameter of each scaffold group was determined by image analysis with at least 300 fibers measured per group. Average fiber diameter ± standard error of the mean (SEM) was reported. Interfiber diameter was calculated by measuring the distance between a fiber and the closest adjacent fiber within the same plane. A minimum of 100 interfiber distances was calculated for each group. Mean interfiber distance ± SEM was reported. Changes in scaffold morphology as a result of exposure to media, were assessed by incubating the scaffolds in media for 1 week with the media exchanged daily. Scaffolds were then rinsed 2×5 min with PBS, a graded alcohol series (50%, 70% for 5 min, followed by 80%, 95%, 100%, and 100% for 10 min), and dried in a graded ethanol:hexamethyldisilazane (HMDS; Ted Pella, Redding, CA) series (3:1, 1:1, and 1:3 for 30 min each, followed by pure HMDS overnight). The dried samples were mounted and examined via scanning electron microscopy as earlier.

Scaffold porosity

The porosity of dry gelatin scaffolds was determined by weighing electrospun disks and calculating the volume of each disk ($n = 8$ per group). The amount of free volume or porosity was then calculated by comparing the density of the electrospun disk to that of a theoretically solid gelatin disk of the same volume.

To quantify if exposure to aqueous media alters scaffold porosity, scaffolds were cross-linked, rinsed, and soaked in HBS for 48 h. Porosity of hydrated gelatin scaffolds was then calculated by measuring pore areas from histological sections. Briefly, scaffolds from each solution concentration were processed, embedded *en face*, and sectioned with 20 μm between sections. The pore area of four distinct areas on 16 sections, each in a different plane of the sample, was assessed via image analysis (Image J). The porosity of the sample was then calculated by multiplying the total pore area by the thickness of the section, which was subsequently divided by the total volume occupied by the section. Mean wet porosity ± SEM was plotted.

Permeability

Permeability of the hydrated scaffolds was defined as the quantity of fluid able to pass through a given volume of scaffold per second. Scaffolds ($n \geq 12$; 24 mm in diameter and 1.5 mm thick) were placed between two meshed

plastic support grids (Nuclepore Filtration Products, Pleasanton, CA), which held the gelatin scaffold in place without compressing it. The mesh screens were placed into the bottom of a clear polypropylene tube which was subsequent filled with 30 mL of medium. The time required for 5 mL of medium to flow through the scaffold, as indicated by volume markings which were scribed onto the tube, was recorded and permeability (K, m/s) of the scaffold calculated as follows using Darcy's Law:

$$K = \frac{Q}{A}\left(\frac{l}{\Delta h}\right)$$

where Q is flow rate (m^3/s), l is sample thickness (m), A is flow area (m^2), and Δh is the change in hydraulic head over l (m).

Cell culture

Human keratinocytes (HK) and fibroblasts (HF) were isolated simultaneously from fresh adult female breast or abdominal skin obtained with Institutional Review Board approval, and cells were grown in selective growth medium.[41] Cells and grafts fabricated from each biopsy were maintained separately (strains 674, 707, and 737). For inoculation, the area of the gelatin scaffolds was calculated by measuring the width and length of the rectangular scaffold (3×9 cm^2). HF (passage 2) were inoculated onto rinsed scaffolds at a density of 5×10^5 cells/cm^2 and incubated at 37°C and 5% CO_2 in cultured skin substitute (UCMC 160) medium.[41] The fibroblast-populated scaffold was incubated in growth media for 1 day. The area of each HF-collagen substrate was measured again and scaffolds were inoculated with HK (passage 2) at a density of 1×10^6 cells/cm^2. The following day (incubation day 1) the HK-HF-gelatin scaffold composites (i.e. electrospun gelatin skin substitute, EGSS) were placed onto a perforated stainless steel platform covered by a cotton pad to establish an air–liquid interface and cultured up to 21 days with the medium replaced daily.

Histology

Biopsies for histology were collected at culture days 7, 14, and 21 and fixed in formalin for 1 h prior to processing and paraffin embedding. Sections were stained with hematoxylin and eosin (H&E) and imaged with light microscopy. Brightfield images were collected with SPOT Advanced imaging software (Diagnostic Instruments, Sterling Heights, MI) with a total of eight specimens per condition per time point. To visualize and quantify the depth of cell penetration, biopsies were collected at day 7 and processed for frozen sections ($n = 9$ per group). Frozen samples were fixed with methanol for 10 min, followed by acetone for 2 min. After fixation, the samples were rinsed 2× with PBS and pretreated for 1 h with PBS containing 2% bovine serum albumin and 2% normal goat serum, followed by incubation overnight at 4°C with the primary antibody for bovine collagen type I (Chemicon International, Temecula, CA). The sections were thoroughly rinsed with PBS then stained with the appropriate secondary antibody for 1 h at room temperature. Disks were subsequently incubated with DAPI (1:5000; Invitrogen, Eugene, OR) for 10 min at room temperature. Negative controls were performed for nonspecific primary binding by incubating sections with a polyclonal rabbit antibody for AQP3 (1:100; Invitrogen, Eugene, OR) which is not present in the ESS and for nonspecific secondary binding by omitting the primary antibody staining and incubating the section in secondary antibody only. After rinsing with PBS and deionized water, the double-labeled sections were examined via epi-fluorescence microscopy (Nikon Microphot FXA, Melville, NY) at 10×. Images were collected with SPOT Advanced imaging software with a total of nine specimens per condition. Depth of penetration was determined by dividing each field of view into five regions and measuring the depth of the deepest penetrating cell per region and the thickness of the collagen in that region. Average values for each field of view were compiled for each sample and the mean % penetration for each group was reported ±SEM.

Surface electrical capacitance measurement

A definitive requirement for the closure and healing of full-thickness skin wounds is the restoration of the epidermal barrier that protects the body from microbial infection and loss of endogenous fluids. Studies have shown that surface electrical capacitance (SEC) can be used as direct, convenient, and inexpensive method to measure skin surface hydration, which is inversely related to barrier function.[42,43] SEC measurements were collected from the EGSS grafts *in vitro* using the NOVA dermal phase meter (DPM 9003; NOVA Technology, Portsmouth, NH). On culture days 7, 14, and 21, measurements were taken from three sites on each ESS (24 grafts per group, 36 measurements total) and the SEC values are expressed in mean pFarads ± SEM. SEC readings from normal human skin were collected from the volar forearm of healthy volunteers.[43]

MTT cell metabolism assay

To evaluate cell metabolism within the constructs, 4-mm punch biopsies were collected from the EGSS at days 7, 14, and 21 (3 punches/graft, 24 grafts total) and each placed into a separate well of a 24-well plate. A modified MTT assay was performed on the biopsy punches. Briefly, 0.5 mL of a sterile filtered solution of 0.5 mg MTT/mL PBS solution was added to each well of a 24-well plate, each containing one 4-mm punch. The biopsies were incubated in the MTT solution for 3 h at 37°C and 5% CO_2. After 3 h, the MTT solution was aspirated from the well and replaced with 0.5 mL methoxyethanol (Fisher Scientific, Fair Lawn, NJ) and agitated on a rocking plate for 3 h to solubilize the formazan crystals. The amount of MTT-formazan product released was measured at 590 nm on a microplate reader with values reported as mean optical density ± SEM.

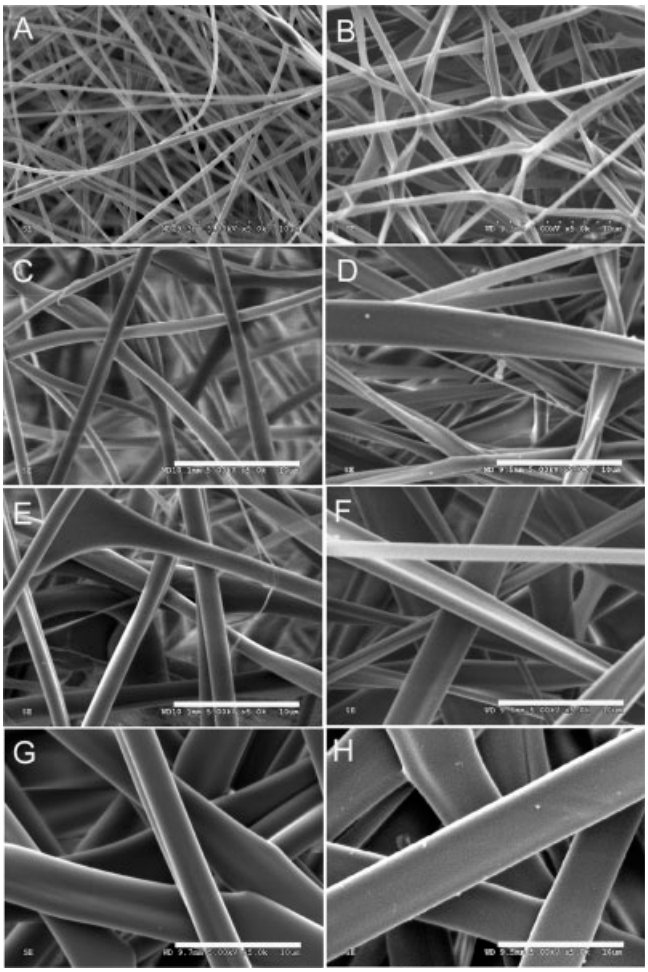

Figure 1. SEM micrographs of electrospun gelatin prior to (A, C, E, F) and after hydration (B, D, F, H). (A, B) 10, (C, D) 12, (E, F) 14, and (G, H) 16 wt/vol % gelatin scaffolds. Scale bar = 10 μm.

Statistical analysis

For quantitative assessments of scaffold physical properties, regression analyses were performed. For quantitative biological assays and the permeability assay, one-way analysis of variance (ANOVA), followed by Tukey-Kramer multiple comparison analysis was performed. The data were presented as mean ± SEM, and $p < 0.05$ was considered statistically significant.

RESULTS

Effect of solution concentration on physical properties

Scanning electron micrographs reveal that the morphology of the electrospun gelatin scaffold changes as a function of solution concentration (Fig. 1). Higher solution concentrations, such as 14 and 16 wt/vol %, are comprised of a lower density of larger fibers [Fig. 1(E–H)] compared with lower solution concentrations [Fig. 1(A–D)]. The morphology of the scaffolds was altered by exposure to medium (Fig. 1). In all groups, fibers swelled with exposure to water, and within the 10% group a large number of fibers which had become fused at their intersections were seen [Fig. 1(B)]. Quantitative assessment of the scanning electron micrographs from as-spun scaffolds supported the observation that fiber diameter increased with solution concentration. The mean fiber diameter in the 10% group was 0.57 ± 0.01 μm, whereas the 16% group had a mean diameter of 3.01 ± 0.06 μm (Fig. 2). Regression analysis showed that solution concentration was a significant predictor for fiber diameter ($p < 0.001$). Fiber density also positively scaled with solution concentration with a max-

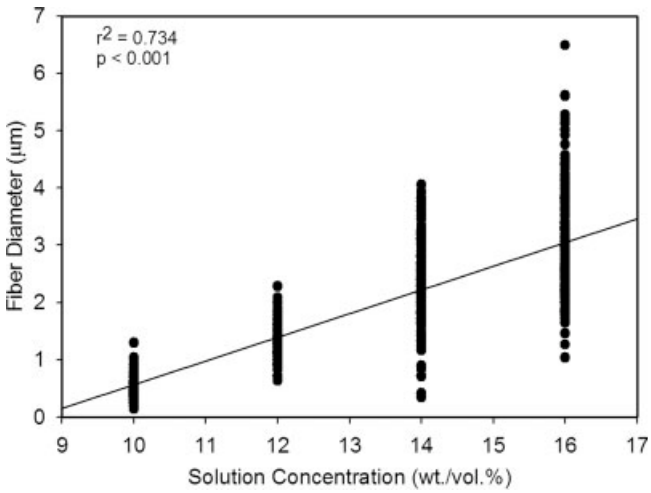

Figure 2. Scatter plot of fiber diameter as a function of electrospinning solution concentration.

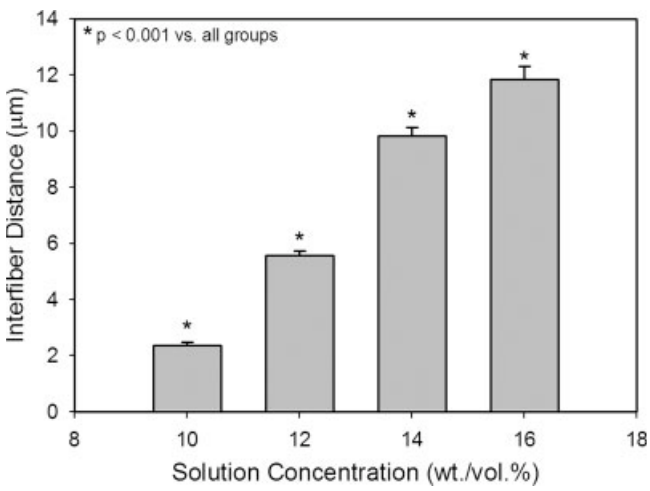

Figure 3. Mean interfiber distance and a function of solution concentration.

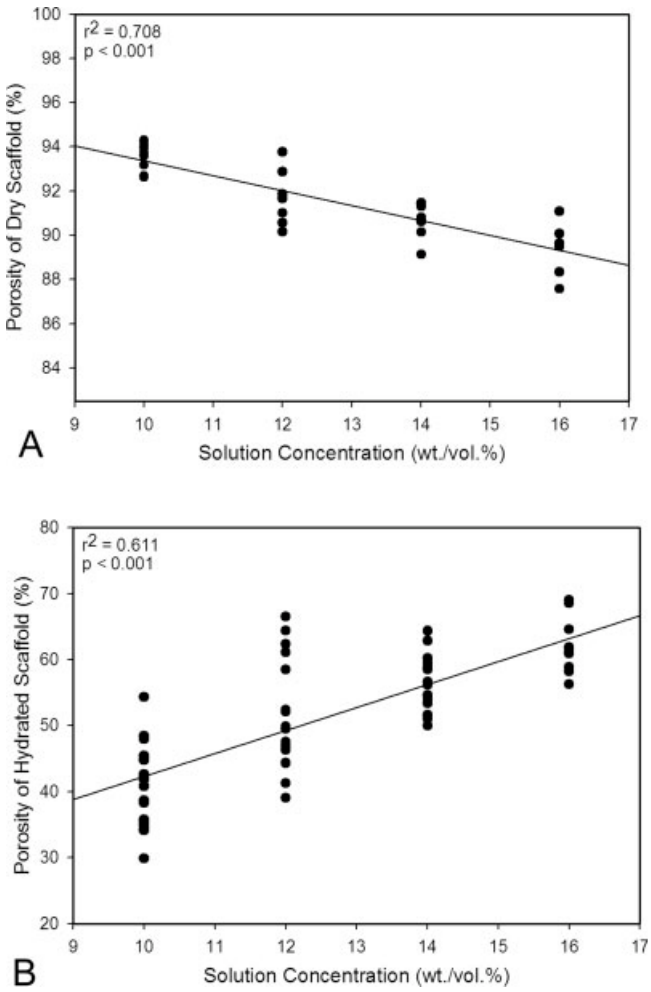

Figure 4. Scatter plot of porosity measurements from (A) dry and (B) hydrated electrospun scaffolds as a function of solution concentration.

imum average interfiber distance of 11.84 ± 0.47 μm occurring in the 16% group (Fig. 3).

Porosity of dry scaffolds was inversely related to scaffold concentration with an average porosity of 93.5% ± 0.2% in the 10% group and 89.3% ± 0.4% in the 16% [Fig. 4(A)]. Exposure to HBS for 48 h significantly reduced scaffold porosity in all groups as revealed by histological evaluation. The relationship between scaffold concentration and porosity was inverted in the hydrated scaffolds [Fig. 4(B)]. The 16% group was the most porous (62.8% ± 1.0%) and the 10% group was the least porous (39.5% ± 1.3%). The porosity of both dry and hydrated scaffolds correlated to solution concentration [Fig. 4(A,B), $p < 0.001$], however, the porosity of the dry scaffolds was more faithfully predicted by solution concentration ($r^2 = 0.708$). Scaffolds fabricated from higher concentration solutions were also more permeable with the 16% group significantly more permeable than all other groups (Fig. 5).

Co-culture of HK and HF on ES gelatin scaffolds

Histological images showed dense populations of fibroblasts present in all groups at days 7, 14, and 21 (day 14; Fig. 6). A thick epithelium with basal keratinocytes was present in the 10, 12, and 14% groups [Fig. 6(A–C)] but not evident in the 16% group. The 16% group was not well stratified and only a thin epithelium existed [Fig. 6(D)]. While fibroblasts were present in all groups, the distribution of fibroblasts was variable and dependent on scaffold morphology. Dense layers of cells in the upper third of the ES gelatin scaffold were present at 10 and 12 wt/vol % gelatin, whereas with 14 and 16%, cells densely occupied the majority of the scaffold (Fig. 7). Negative controls revealed low levels of nonspecific binding of the primary antibody to the epidermis only. Thus, the gelatin scaffolds were identified by both positive staining for collagen and by morphology which is distinct in structure from the epidermis (Fig. 7, white dashed line). Cells within the 10% scaffold penetrated 61.99% ± 3.195% of the collagen sponge, whereas cells within the 16% scaffold penetrated the scaffold to significantly greater extent (85.18% ± 2.447%, $p < 0.001$). The 12% scaffold did not enhance cell penetration (63.55% ± 2.953%) compared with the 10% and cells penetration within this scaffold was significantly impeded compared with the 14% (75.48% ± 2.958%) and 16% ($p < 0.05$).

As the ESS matured at the air–liquid interface, the epithelium keratinized (Fig. 6, arrows), began to form an epidermal barrier, and caused the surface of the material to dry. SEC measurements on all groups at day 7 revealed that the surface of the skin substitutes was still moist and had not yet fully matured. By day 14, the expected reduction in surface hydration occurred in all groups, with the least reduction

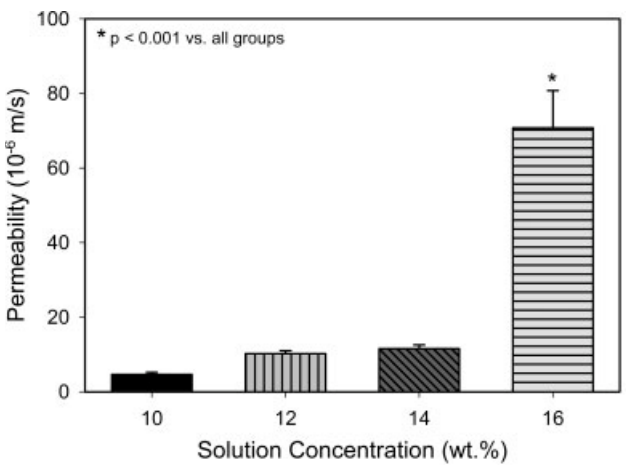

Figure 5. Permeability of hydrated gelatin scaffolds. Note significant increase in scaffold permeability in the 16% group.

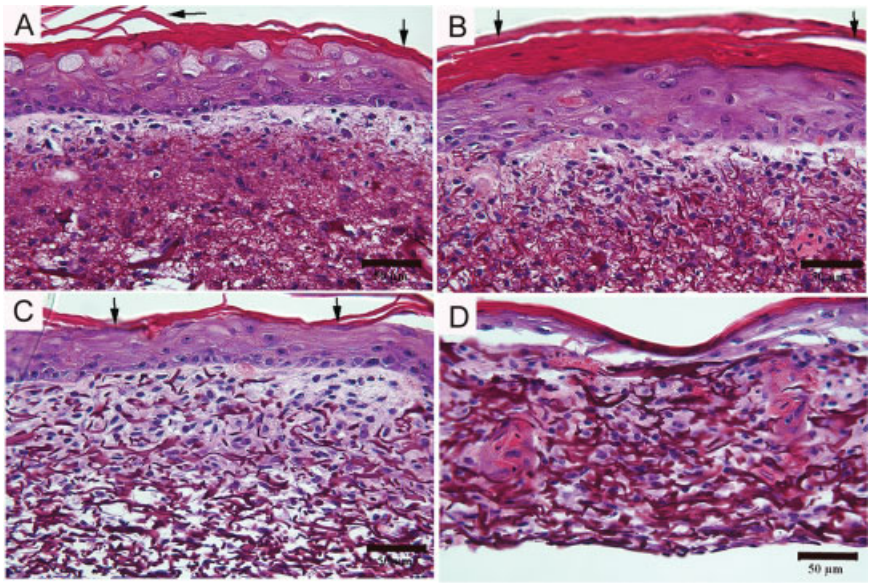

Figure 6. H&E stained cross-sections of skin substitutes made with (A) 10, (B) 12, (C) 14, and (D) 16 wt/vol % gelatin scaffolds after 14 days in culture. Note the well-stratified dermal and epidermal layers in the 10, 12, and 14% groups and lack of a well-formed epidermis in the 16 wt % group. Arrows point to cornified layers formed in the 10, 12, and 14% group. Scale bar = 50 μm.

seen in the 16% group (Fig. 8). After culturing for 21 days at the air–liquid interface, all groups, except 16%, were within normal human skin levels (Fig. 8). The 16% group did not undergo normal barrier formation as evidenced by high SEC levels at day 21. These results correspond to histological images where only a thin epithelium lacking stratification was present [Fig. 6(D)].

Analysis of cell metabolism via MTT revealed a statistically significant difference in cell metabolism between the 12% group and the 16% group at day 7 ($p < 0.05$; Fig. 9). By day 14, the 10, 12, and 14% groups had significantly higher MTT values than the 16% group ($p < 0.05$; Fig. 9). At day 21, the 12% group had the highest average MTT value which was statistically different than the 14 and 16% group.

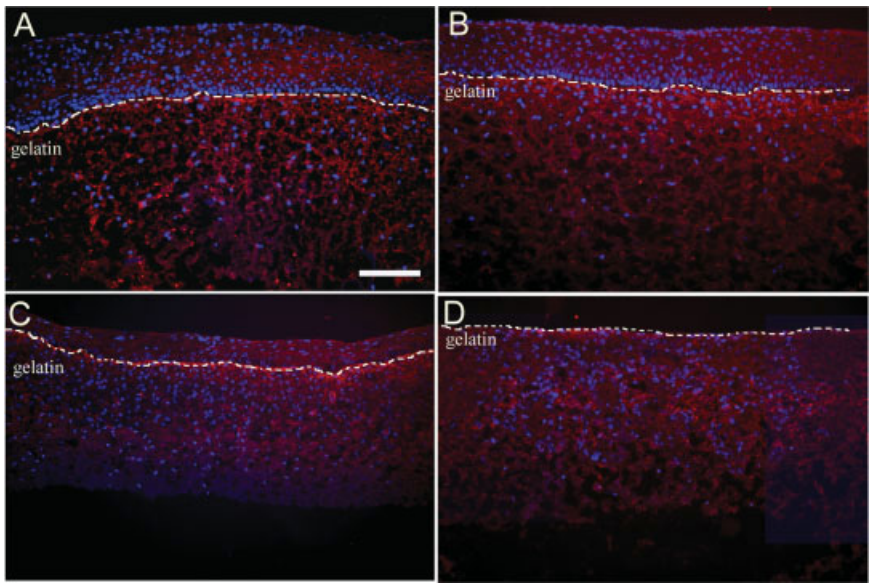

Figure 7. Immunostained cross-sections of EGSS made with (A) 10, (B) 12, (C) 14, and (D) 16 wt/vol % gelatin scaffolds after 7 days in culture. Red = collagen; blue = cell nuclei. Gelatin scaffolds were identified by both positive staining for collagen and morphology. The upper surface of the gelatin scaffold is marked by the white dashed line. Note the high density of cells present on the surface and in the upper portions of the collagen scaffold on the 10 and 12% (A, B) groups compared with the more even distribution of cells throughout the scaffold in the 14 and 16% groups (C, D). Scale bar = 50 μm.

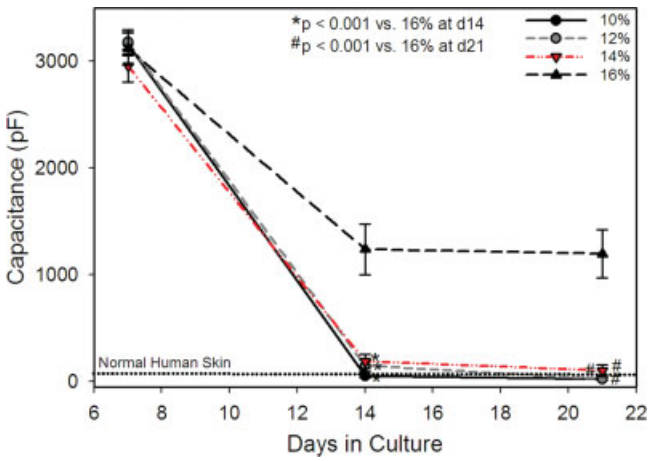

Figure 8. Surface hydration measurements at days 7, 14, and 21. By day 14, the 10, 12, and 14 wt % groups have approached normal human skin (NHS) SEC levels. [Color figure can be viewed in the online issue, which is available at www.interscience.wiley.com.]

These results were consistent with the histological images, which showed much smaller populations of keratinocytes on the 16% gelatin scaffolds.

DISCUSSION

Physical characterization of electrospun gelatin scaffolds reveals that altering solution concentration is an effective method for controlling scaffold morphology. Several other factors can control electrospun scaffold morphology including feed velocity of the solution, electric potential at the tip, distance from the tip and the target, temperature, humidity, and air velocity in the chamber.[44–46] However, solution concentration is an easily controlled variable to alter fiber diameter and porosity.

The quantitative data presented here demonstrate that there are direct relationships among fiber diameter, interfiber distance, and porosity of the hydrated scaffold with large fiber diameters associated with greater interfiber distances and porosities. Porosity measurements of the hydrated scaffolds, in addition to the as-spun material, are of particular interest as the scaffolds may experience significant reductions in porosity after exposure to aqueous media. The significant loss of porosity when hydrated could be due to swelling and partial degradation of the gelatin fibers. For example, Zhang et al. reported partial degradation and swelling of glutaraldehyde vapor crosslinked gelatin nanofibers when exposed to deionized water at 37°C for up to 6 days.[5] The higher surface area to volume ratio of thinner fibers allows them to swell more rapidly than the more robust fibers and allows fibers to fuse at their junctions, which was observed presently [Fig. 1(B)] and in other studies.[5] This process could have lead to the larger percent decrease in porosity upon hydration in the 10% (56.4%) compared with the 16% group (30.3%).

Nutrient influx to cells and waste elimination are crucial to any tissue. Cells *in vivo* rely on proximity of blood capillaries for most of their mass transport requirements. Cell-populated constructs *in vitro* have no inherent nutrient supply from blood vessels, relying instead on diffusion for cell survival.[47,48] Scaffold permeability can greatly affect the ability of nutrients and metabolites to diffuse through the collagen substrate to the cells. Gelatin scaffolds fabricated from 16% solutions were highly permeable (0.0007 m^2/s; Fig. 5) when compared with the other groups. High levels of porosity, larger interfiber distances, and larger fiber diameters are all factors that lead to greater permeability. Medium can easily filter through a more porous scaffold with increased interfiber distances where the path of the medium is less tortuous. The low surface area to volume ratio of the larger fiber also generates less fiber swelling and fiber degradation, which medium to more free space through which medium can pass. However, cell metabolism on scaffolds with large fiber diameters and interfiber distances was reduced in comparison to more dense scaffolds, which appears to contradict the permeability results. Histologic evaluation of the scaffolds indicated that there were lesser populations of cells on the 14 and 16% scaffolds. Thus, the reduced cell metabolism in the 14 and 16% groups at day 21 is not likely a result of poor nutrient influx and waste elimination but rather due to lower cell number.

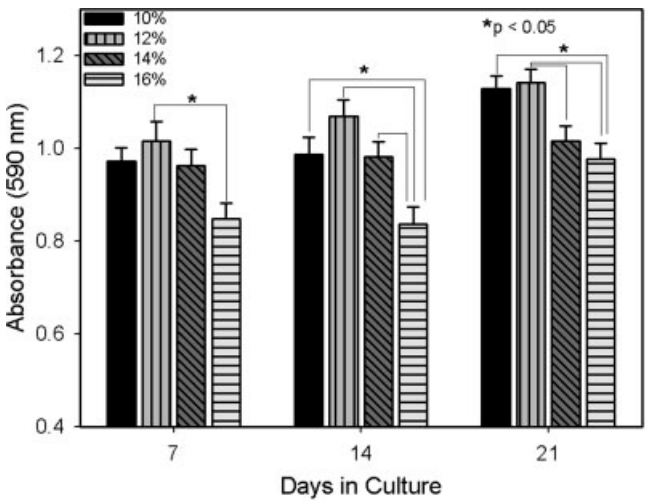

Figure 9. MTT assay of cell metabolism in skin substitutes made with electrospun gelatin scaffolds at culture days 7, 14, and 21. Note significant difference decrease in cell metabolism in the 16% group versus the 12% group at all time points.

The application of cultured human fibroblasts and keratinocytes to gelatin scaffolds reveals that all scaffolds are capable of sustaining cell growth and attachment. A MTT assay was utilized to determine cell metabolism within these constructs. As there are two cell types within the scaffold with different levels of metabolism in the culture media, a calibration curve for absolute cell numbers would be challenging and likely inaccurate. These difficulties could be increased due to differences in cell attachment, proliferation, or mortality, and thus values for cell metabolism were not extrapolated to absolute cell numbers. The 16% scaffolds have the lowest average cell metabolism at all time points. It is possible that, because the scaffolds are highly permeable and porous, a percentage of the cell inoculum filtered through the scaffolds without allowing sufficient time for cell attachment. The distribution of fibroblasts in the deeper portions matrix indicated that it is possible that a small percentage of cells either passed directly through the scaffold or did not have sufficient time to attach. The percentage of attached cells has previously shown to be inversely correlated to pore size.[29] The lack of a thick epithelium and a basal keratinocyte cell layer in the 16% groups may also explain the low MTT values as the CK account for roughly 67% of the initial cell population per cm^2 and the keratinocytes are more metabolically active than the fibroblasts in this model.

Cellular organization and maturation are essential to development of composite dermal–epidermal substitutes that will be effective for wound healing. The formation of a thick, well-stratified epithelium is a key functional component of a skin substitute and is essential to wound closure as it provides a barrier to fluid loss and infection. However, a well-formed epidermis is dependent on a viable, well-populated dermis. Thus, to provide the greatest benefits to patients both the dermal and epidermal components need to be viable and well organized. Presently, scaffold morphology appears to control the organization of skin substitutes with both dermal and epidermal components. Electrospun scaffolds with a mean interfiber distance of 9.8 μm or less demonstrated organized dermal and epidermal layers. Interfiber diameters greater than this are associated with poorly formed epithelium. Large interfiber distances allow cells to infiltrate the scaffold easily; however, there appears to be some critical value over which the fibroblasts do not form a dense continuous layer. Cells were inoculated onto scaffolds based on surface area, not volume. It is possible that as cell penetration increases, as seen in the 16% group, the density of cells decreases because they are occupying a larger volume of scaffold. Fibroblasts would then not form a continuous cell sheet upon which the keratinocytes can attach. The poorly formed epidermal layer seen in the 16% group correlates with a failure to form an epidermal barrier as seen in the high SEC values in Figure 7.

CONCLUSIONS

Electrospun gelatin scaffolds can be used as a surrogate ECM for dermal tissue regeneration. The physical properties of the scaffold, principally porosity and interfiber distance, play a significant factor in tissue morphogenesis. Fibers that are spaced greater than 10 μm apart appear to allow too much initial cell penetration, preventing fibroblasts from densely occupying the upper portion of the scaffold to generate a dense layer upon which keratinocytes can attach. Interfiber distances between 5 and 10 μm appear to possess the preferred set of properties including high cell viability, optimal cell organization, and excellent barrier formation. Therefore, dermal substitutes fabricated from electrospun gelatin have the potential to be therapeutic clinically and may provide wound healing more efficiently than the conventional techniques.

The authors thank Dr. David Witte within the Department of Pathology at the Cincinnati Children's Hospital Medical Center for the use of their scanning electron microscopy facilities.

References

1. O'Brien F, Harley B, Yannas I, Gibson L. Influence of freezing rate on pore structure in freeze-dried collagen-GAG scaffolds. Biomaterials 2004;25:1077–1086.
2. Matthews JA, Wnek GE, Simpson DG, Bowlin GL. Electrospinning of collagen nanofibers. Biomacromolecules 2002;3: 232–238.
3. Zhang YZ, Ouyang HW, Lim CT, Ramakrishna S, Huang ZM. Electrospinning of gelatin fibers and gelatin/PCL composite fibrous scaffolds. J Biomed Mater Res B Appl Biomater 2005;72:156–165.
4. Lu QJ, Ganesan K, Simionescu DT, Vyavahare NR. Novel porous aortic elastin and collagen scaffolds for tissue engineering. Biomaterials 2004;25:5227–5237.
5. Zhang Y, Venugopal J, Huang Z-M, Lim C, Ramakrishna S. Crosslinking of the electrospun gelatin nanofibers. Polymer 2006;47:2911–2917.
6. Ulubayram K, Cakar A, Korkusuz P, Ertan C, Hasirci N. EGF containing gelatin-based wound dressings. Biomaterials 2001; 22:1345–1356.
7. Neumann P, Zur B, Ehernreich Y. Gelatin-based sprayable foam as a skin substitute. J Biomed Mater Res 1981;15:9–18.
8. Wang T-W, Wu H-C, Huang Y-C, Sun J-S, Lin F-H. Biomimetic bilayered gelatin-chondroitin 6 sulfate-hyaluronic acid biopolymer as a scaffold for skin equivalent tissue engineering. Artif Organs 2006;30:141–149.
9. Lee S, Kim Y, Chong M, Hong S, Lee Y. Study of gelatin-containing artificial skin. V. Fabrication of gelatin scaffolds using salt-leaching method. Biomaterials 2005;26:1961–1968.

10. Choi Y, Hong S, Lee Y, Song K, Park M, Nam Y. Studies on gelatin-containing artificial skin. II. Preparation and characterization of cross-linked gelatin-hyaluronate sponge. J Biomed Mater Res B Appl Biomater 1999;48:631–639.
11. Choi Y, Hong S, Lee Y, Song K, Park M, Nam Y. Study on gelatin-containing artificial skin. I. Preparation and characteristics of novel gelatin–alginate sponge. Biomaterials 1999;20: 409–417.
12. Choi Y, Lee S, Hong S, Lee Y, Song K, Park M, Nam Y. Studies on gelatin-based sponges, Part 3: A comparative study of cross-linked gelatin/alginate, gelatin/hyaluronate and chitosan/hyaluronate sponges and their application as wound dressings in full-thickness skin defect of rat. J Mater Sci Mater Med 2001;12:67–73.
13. Reneker D, Kataphinan W, Theron A, Zussman E, Yarin A. Nanofiber garlands of polycaprolactone by electrospinning. Polymer 2002;45:6785–6794.
14. Huang Z-M, Zhang Y, Kotaki M, Ramakrishna S. A review on polymer nanofibers by electrospinning and their applications in nanocomposites. Compos Sci Technol 2003;63:2223–2253.
15. Li M, Mondrinos MJ, Gandhi MR, Ko FK, Weiss AS, Lelkes PI. Electrospun protein fibers as matrices for tissue engineering. Biomaterials 2005;26:5999–6008.
16. Li M, Mondrinos MJ, Chen X, Gandhi MR, Ko FK, Lelkes PI. Co-electrospun poly(lactide-*co*-glycolide), gelatin, and elastin blends for tissue engineering scaffolds. J Biomed Mater Res A 2006;79:963–973.
17. Telemeco TA, Ayres C, Bowlin GL, Wnek GE, Boland ED, Cohen N, Baumgarten CM, Mathews J, Simpson DG. Regulation of cellular infiltration into tissue engineering scaffolds comprised of submicron diameter fibrils produced by electrospinning. Acta Biomater 2005;1:377–385.
18. Glicklis R, Shapiro L, Agabaria R, Merchuk J, Cohen S. Hepatocyte behavior within three-dimensional porous alginate scaffolds. Biotechnol Bioeng 2000;67:344.
19. Ma T, Li Y, Yang S-T, Kniss D. Effects of pore size in 3-D fibrous matrix on human trophoblast tissue development. Biotechnol Bioeng 2000;70:606–618.
20. Wang H, Pieper J, Peters F, van Blitterswijk C, Lamme E. Synthetic scaffold morphology controls human dermal connective tissue formation. J Biomed Mater Res A 2005;74:523–532.
21. Salem A, Stevens R, Pearson R, Davies M, Tendler S, Roberts C, Williams P, Shakesheff K. Interaction of 3T3 fibroblasts and endothelial cells with defined pore features. J Biomed Mater Res 2002;61:212–217.
22. LiVecchi AB, Tombes RM, LaBerge M. In vitro chondrocyte collagen deposition within porous HDPE: Substrate microstructure and wettability effects. J Biomed Mater Res 1994;28: 839–850.
23. Nehrer S, Breinan H, Ramappa A, Young G, Shortkroff S, Louie L, Sledge C, Yannas I, Spector M. Matrix collagen type and pore size influence behaviour of seeded canine chondrocytes. Biomaterials 1997;18:769–776.
24. Kuberka M, von Heimberg D, Schoof H, Heschel I, Rau G. Magnification of the pore size in biodegradable collagen sponges. Int J Artif Organs 2002;25:67–72.
25. Khil M-S, Bhattarai S, Kim H-Y, Kim S-Z, Lee K-H. Novel Fabricated matrix via electrospinning for tissue engineering. J Biomed Mater Res B Appl Biomater 2005;72:117–124.
26. van Tienen T, Heijkants R, Buma P, deGroot J, Pennings A, Veth R. Tissue ingrowth and degradation of two biodegradable porous polymers with different porosities and pore sizes. Biomaterials 2002;23:1731–1738.
27. Yannas I, Lee E, Orgill D, Skrabut E, Murphy G. Synthesis and characterization of a model extracellular matrix that induces partial regeneration of adult mammalian skin. Proc Natl Acad Sci USA 1989;86:933–937.
28. Noh H, Lee S, Kim J-M, Oh J-E, Kim K-H, Chung C-P, Choi S-C, Park W, Min B-M. Electrospinning of chitin nanofibers: Degradation behavior and cellular response to normal human keratinocytes and fibroblasts. Biomaterials 2006;27:3934–3944.
29. O'Brien F, Harley B, Yannas I, Gibson L. The effect of pore size on cell adhesion in collagen-GAG scaffolds. Biomaterials 2005;26:433–441.
30. Noah E, Chen J, Jiao X, Heschel I, Pallua N. Impact of sterilization on the porous design and cell behavior in collagen sponges prepared for tissue engineering. Biomaterials 2002;23:2855–2861.
31. Tsuruga E, Takita H, Itoh H, Wakisaka Y, Kuboki Y. Pore size of porous hydroxyapatite as the cell-substratum controls BMP-induced osteogenesis. J Biochem 1997;2:317–324.
32. Doillon C, Whyne C, Brandwein S, Silver F. Collagen-based wound dressings: Control of the pore structure and morphology. J Biomed Mater Res 1986;8:1219–1228.
33. Boyce ST, Hansbrough JF. Biologic attachment, growth and differentiation of cultured human epidermal keratinocytes on a graftable collagen and chondroitin-6-sulfate substrate. Surgery 1988;103:421–431.
34. Yannas IV, Burke JF. Design of an artificial skin. I. Basic design principles. J Biomed Mater Res 1980;14:65–81.
35. Heimbach D, Luterman A, Burke JF, Cram A, Herndon D, Hunt J. Artificial dermis for major burns: A multi-center randomized clinical trial. Surgery 1988;208:313–320.
36. Hansbrough JF, Boyce ST, Cooper ML, Foreman TJ. Burn wound closure with cultured autologous keratinocytes and fibroblasts attached to a collagen–glycosaminoglycan substrate. JAMA 1989;262:2125–2130.
37. Boyce ST, Kagan RJ, Greenhalgh DG, Warner P, Yakuboff KP, Palmieri T, Warden GD. Cultured skin substitutes reduce requirements for harvesting of skin autograft for closure of excised, full-thickness burns. J Trauma 2006;60:821–829.
38. Erdag G, Sheridan R. Fibroblasts improve performance of cultured composite skin substitutes on athymic mice. Burns 2004;30:322–328.
39. Freyman TJ, Yannas IV, Yokoo R, Gibson LJ. Fibroblasts contraction of a collagen-GAG matrix. Biomaterials 2001;22:2883–2891.
40. Yannas IV. Collagen, gelatin in the solid state. Rev Macromol Chem 1972;C7:49–104.
41. Swope VB, Supp AP, Schwemberger S, Babcock G, Boyce S. Increased expression of integrins and decreased apoptosis correlate with increased melanocyte retention in cultured skin substitutes. Pigment Cell Res 2006;19:424–433.
42. Boyce ST, Supp AP, Harriger MD, Pickens WL, Hoath SB. Surface electrical capacitance as a noninvasive index of epidermal barrier in cultured skin substitutes in athymic mice. J Invest Dermatol 1996;107:82–87.
43. Goretsky M, Supp AP, Greenhalgh DG, Warden GD, Boyce S. Surface electrical capacitance as an index of epidermal barrier properties of composite skin substitutes and skin autografts. Wound Repair Regen 1995;3:419–425.
44. Chew SY, Wen Y, Dzenis, Y, Leong KW. The role of electrospinning in the emerging field of nanomedicine. Curr Pharm Des 2006;12:4751–4770.
45. Reneker DH, Chun I. Nanometer diameter fibers of polymer, produced by electrospinning. Nanotechnology 1996;7:216–223.
46. Deitzel J, Kleinmeyer J, Hirvonen J, Beck Tan N. Controlled deposition of electrospun poly(ethylene oxide) fibers. Polymer 2001;42:8163–8170.
47. Bursac N, Freed L, Biron R, Vunjak-Novakovic G. Mass transfer studies of tissue engineered cartilage. Tissue Eng 1996;2: 141–150.
48. Karande TS, Ong JL, Agrawal CM. Diffusion in musculoskeletal tissue engineering scaffolds: Design issues related to porosity, permeability, architecture, and nutrient mixing. Ann Biomed Eng 2004;32:1728–1743.